Fermi Surface and Magnetic Structure of $TmGa_3$

M. Biasini,[1,*] G. Kontrym-Sznajd,[2] M. A. Monge,[1,†] M. Gemmi,[1] A. Czopnik,[2] and A. Jura[2]

[1]*ENEA, Via Don Fiammelli 2, 40129 Bologna, Italy*

[2]*Trzebiatowski Institute of Low Temperature and Structure Research, P.O. Box 937, Wroclaw, Poland*

(Received 14 November 2000)

We carry out measurements of the two-dimensional angular correlation of the positron annihilation radiation (2D-ACAR) to reconstruct the complex multisheet Fermi surface (FS) of the cubic rare-earth (RE) compound $TmGa_3$. We discover a correlation between the antiferromagnetic structures and the nesting of the FS along the [110] directions. Moreover, we propose methods to estimate the density of states at the Fermi energy (E_F) and the electronic contribution to the specific heat [we obtain $N(E_F) = 13.6$ states/Ryd cell and $\gamma = 2.4$ mJ/mole K^2].

DOI: 10.1103/PhysRevLett.86.4616 PACS numbers: 71.18.+y, 75.10.Lp, 78.70.Bj

It is generally accepted that the collective behavior of the magnetic rare-earth (RE) ions in intermetallic compounds is determined by an indirect interaction among localized f electrons, which are coupled by the conduction electrons according to the Ruderman-Kittel-Kasuya-Yosida (RKKY) theory [1]. It has been argued that the Fermi surface (FS) topology might control the magnetic properties of these systems when large parts of the FS can be superimposed through the translation of a single vector $\boldsymbol{q}_0$. This occurrence, denoted as FS nesting, should generate a peak at $\boldsymbol{q}_0$ in the generalized Fourier transformed magnetic susceptibility $\chi(\boldsymbol{q})$, thus favoring the magnetic structure with propagation wave vector $\boldsymbol{q}_0$ [2]. The FS nesting belongs to a class of similar mechanisms, all depending on the shape and the size of the FS, which have been invoked to explain a variety of phenomena, such as antiferromagnetism, spin or charge density waves, Kohn anomalies, Friedel oscillations, RKKY oscillations due to magnetic impurities, and oscillatory coupling in metallic magnetic multilayers. It is worth noticing that the RKKY interaction mentioned above, assuming a constant interaction between the conduction and local $4f$ electrons (k-f), neglects any $\boldsymbol{q}$ dependence in the exchange integral J_{k-f} (which is very difficult to calculate in real cases [3]). Therefore, it is important to test whether the link between FS nesting and magnetism in RE-based compounds is limited to sporadic cases or is general in nature.

An example of a RE system where, to date, there has been no attempt to explain its magnetic properties in terms of the FS topology is provided by $TmGa_3$. The interest in this compound arises from the interplay between antiferromagnetic ordering, antiferroquadrupolar ordering, and crystal electric field which generate a complex low temperature phase diagram ($T_N = 4.26$ K, $T_Q = 4.29$ K) [4–6]. The magnetic structure can be described with propagation vectors from the [110] star. The FS topology of TmGa3, crystallizing in the cubic $AuCu_3$-type structure (space group $Pm3m$) with lattice constant $a = 4.196$ Å, was calculated using the linear-muffin-tin orbital (LMTO) method in local density approximation (LDA) and studied with the de Haas van Alphen (dHvA) experiment [6]. A reasonable agreement between dHvA measurements and *ab initio* calculation was obtained by constraining the $4f$ electrons to retain a local atomic character, i.e., not allowing the $4f$ shell to hybridize with the conduction electrons [6]. This method (denoted as f-core LDA) is also consistent with photoemission studies, which showed that the energy of the $4f^{12}$ states lies 5 eV below E_F [7]. Figure 1a shows the intersection of the FS resulting from the spin polarized f-core LDA calculation performed in Ref. [6] with the high symmetry planes of the cubic BZ. The electronlike part of the FS (from band 7) is a simple spheroidal pocket centered at the R points. Conversely, the holelike part of the FS (from band 6) is a complicated, multiply connected, structure surrounding the X points and the Γ point. Since $TmGa_3$ is a compensated metal, the volume enclosed by the electronlike FS equals that of the holelike. As the dHvA experiment provides only evaluations of the *extremal cross sectional areas* of the FS perpendicular to an applied magnetic field, the nesting properties of the FS could not be investigated. Conversely, the 2D-ACAR measurement, yielding to some extent a

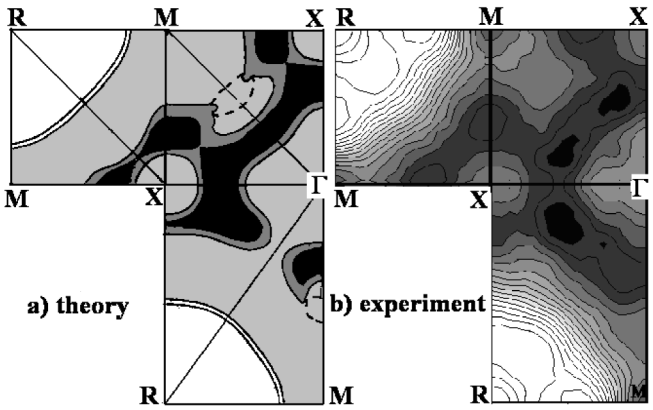

FIG. 1. (a) Sections of the calculated FS of $TmGa_3$ for the spin up and spin down bands in high symmetry planes of the BZ [6]. The white region centred at the R points includes the occupied states of band 7, and the black region includes the unoccupied states of band 6. (b) Experimental $\rho^{ep}_{\mathrm{LCW}}(\boldsymbol{k})$ along the same high symmetry planes as (a).

 0031-9007/01/86(20)/4616(4)$15.00

direct view of the FS, is quite suitable to this purpose. This experiment, by measuring the distribution $N(\theta_x, \theta_y)$ of the deviation angles from anticollinearity of the annihilation γ rays, determines a two-dimensional (2D) projection of the 3D electron-positron (ep) momentum density, $\rho^{ep}(\boldsymbol{p})$ [8]. The contribution to $\rho^{ep}(\boldsymbol{p})$ from the conduction bands l is discontinuous at points $\boldsymbol{p}_{F_l} = (\boldsymbol{k}_{F_l} + \boldsymbol{G})$, where $\boldsymbol{G}$ is a reciprocal lattice vector and $\boldsymbol{k}_{F_l}$ are the reduced Fermi wave vectors in the first Brillouin zone (BZ). The standard Lock-Crisp-West (LCW) transformation [9], extensively used in the data analysis of the 2D-ACAR spectra, reinforces these discontinuities by folding the momentum distribution $\rho^{ep}(\boldsymbol{p})$ back onto the first BZ by translation over the appropriate vectors $\boldsymbol{G}$. If the summation is performed over a sufficient portion of momentum space, the result, denoted here as $\rho^{ep}_{\mathrm{LCW}}(\boldsymbol{k})$, is defined as [10],

$$\rho^{ep}_{\mathrm{LCW}}(\boldsymbol{k}) = \sum_n \theta(E_F - \epsilon_{k,n}) \int |\psi^n_k(\boldsymbol{r})|^2 |\phi(\boldsymbol{r})|^2 g(\boldsymbol{r})\, d\boldsymbol{r}\,. \tag{1}$$

Here ϕ denotes the positron wave function, $\epsilon_{k,n}$ is the energy eigenvalue of the electron from band n with Bloch wave vector $\boldsymbol{k}$ and wave function $\psi^n_{\boldsymbol{k}}$. The factor $g(\boldsymbol{r})$ accounts for the ep correlations [11]. In general, although the mapping of the FS is facilitated when the overlap integral in Eq. (1) is a weakly varying function of $\boldsymbol{k}$, the FS discontinuities [marked by the step function of Eq. (1)] are not shifted by this $\boldsymbol{k}$ dependence [12]. In practice, to obtain the 3D image of the FS, it is necessary to reconstruct the 3D $\rho^{ep}(\boldsymbol{p})$ from its 2D projections using tomographic techniques and then perform the 3D LCW folding.

In this Letter, we provide an accurate description of the FS topology of $TmGa_3$. The results are compared to the dHvA experiment by extracting from our Fermi volume the dHvA frequencies (F_{dHvA}). Moreover, we propose a method to obtain from the 2D-ACAR experiment the electronic part of the specific heat. Finally, we correlate the magnetic properties of $TmGa_3$ with the nesting of the FS in the [110] direction.

The $TmGa_3$ single crystals were grown by the molten-metal solution method. The melt, of composition 90 at. % Ga and 10 at. % Tm, was cooled at the slow rate of 0.8 °C/h from 900 °C to 280 °C and then cooled rapidly down to room temperature to avoid $TmGa_6$ formation. The purities of the substrates were $3N$ and $6N$ for Tm and Ga, respectively. This procedure yielded single crystals of stoichiometric composition immersed in an excess of pure gallium which could easily be removed. The high quality of the crystals was proven by x-ray examination and dHvA measurements. The 2D-ACAR experiments were carried out in the paramagnetic phase with a new setup based on a pair of Anger cameras and described in detail in Ref. [13]. The three projections collected, each amounting to $\approx 2 \times 10^8$ raw coincidence counts, had integration directions (perpendicular to the [001] axis) at 0°, 22.5°, and 45° from the [100] direction. The measurements were performed in a He closed-cycle cryostat at the temperature of 60 K in a vacuum of 1×10^{-6} torr. The estimated overall experimental resolution was equivalent to ≈13% of the BZ size. Next, after applying the Van Citter-Gerhardt deconvolution algorithm [14], the ep momentum density $\rho^{ep}(\boldsymbol{p})$ was reconstructed by the Cormack's [15,16] and modified filtered-back-projection (FBP) [17] algorithms. Both methods exploit the crystal symmetry and can provide a faithful reconstruction of $\rho^{ep}(\boldsymbol{p})$ from a small number of projections, depending on the amount of its anisotropy [18]. In this case three projections proved to be adequate. As the final 3D-LCW [9] transformation applied to $\rho^{ep}(\boldsymbol{p})$ reconstructed using the two methods provided very similar LCW densities $\rho^{ep}_{\mathrm{LCW}}(\boldsymbol{k})$, only Cormack's results will be shown. Figure 1b shows slices of $\rho^{ep}_{\mathrm{LCW}}(\boldsymbol{k})$ along high symmetry planes of the BZ. The broad maxima in the regions centred at the R points of the BZ are in good agreement with the electronlike spheroidal FS (from band 7) predicted by the theory (see Fig. 1a). The high amplitude variation of $\rho^{ep}_{\mathrm{LCW}}(\boldsymbol{k})$ at the $\boldsymbol{k}$ loci of the half maximum of these regions (at $k \sim \overline{XR}/2$ in Fig. 1b) gives little uncertainty about the position of the related spheroidal FS (not shown here). Moreover, the further structure in the regions surrounding the Γ and X points is similar to the occupancy of the theoretical holelike Fermi volume from band 6 (compare Figs. 1b and 1a). It appears that the contribution to $\rho^{ep}_{\mathrm{LCW}}(\boldsymbol{k})$ from the $\boldsymbol{k}$ states related to the holelike Fermi volume (band 6) is less sharp and intense than the corresponding ones from band 7. We attribute this difference to the lower dispersion of band 6 (at the corresponding k_F points the theory [6] predicts $|\nabla\epsilon(k)| \simeq$ 21 eV/a.u. and $|\nabla\epsilon(k)| \simeq 13$ eV/a.u. for bands 7 and 6, respectively). The consequent higher delocalization of the conduction electrons of band 7 increases their overlap with the positron which resides prevalently in the interstices. As the moderate slope of $\rho^{ep}_{\mathrm{LCW}}(\boldsymbol{k})$ at the loci of the half maximum of the holelike structure gave a higher uncertainty concerning the position of the related Fermi edge, we selected the isodensity surface which yielded the closest volume to the electronlike part of the FS. The Fermi volumes obtained correspond to (21 ± 2)% and (26 ± 3)% of the BZ for the electronlike FS and the holelike FS, respectively. Figure 2 shows the complex structure attributed to the holelike FS. The main discrepancy with the theory [6] consists in the absence of the interruption of the FS in the ΓR direction (see Fig. 1a, where, on going from Γ to R, only the Fermi edge due to band 7 is found, unlike the experimental case shown in Fig. 1b). The discrepancy could be due to insufficient instrumental resolution. On the other hand, the small FS features surrounding the X points (see Figs. 1 and 2), could be recovered after the application of our deconvolution procedure. The FS sizes along high symmetry directions obtained from reconstructed $\rho^{ep}_{\mathrm{LCW}}(\boldsymbol{k})$ and calculated FS [6] are shown in Table I.

These results were compared to the dHvA experiment. To do so, we generated the angular dependence of the

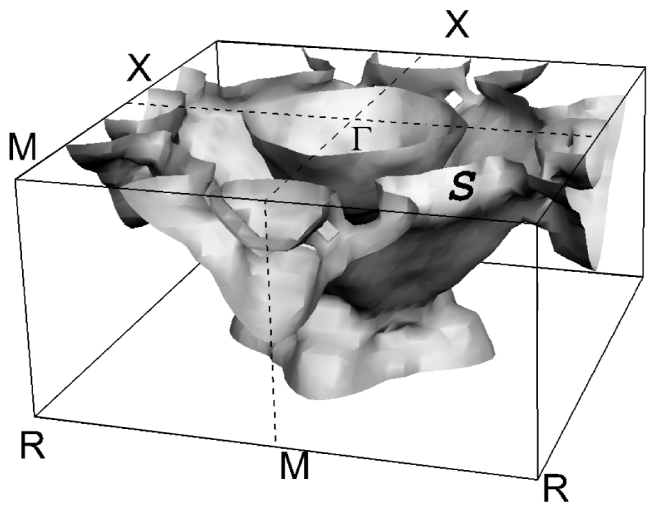

FIG. 2. Experimental holelike FS for $TmGa_3$ shown in half BZ. The unoccupied region lies between the inner surface, centered at Γ and X, and the outer surface. The nesting part of the FS (see text) is denoted by letter S.

extremal cross sectional areas (transformed into F_{dHvA} frequencies) of the electronlike and holelike FS sheets. Figure 3 shows the generated and experimental (dHvA) frequencies [6]. The shape of our angular dependence turns out to be rather insensitive to the values of $\rho^{ep}_{\mathrm{LCW}}(\boldsymbol{k})$ selected (once and for all) for the isocontour sections. The branches denoted by α and δ in Fig. 3 are in good agreement with the experimental ones [6]. However, contrary to our results, we note that one β branch (see arrows in Fig. 3), attributable to the holelike FS, is interrupted when the magnetic field, $\boldsymbol{B}$, is parallel to [110], in agreement with the theoretical occupancy in the ΓR direction (see Fig. 1a [6]). Moreover, the dHvA low-frequency signals were not reproduced by our method (the same discrepancy was obtained by the LMTO calculation [6]).

Next, we derived figures for the electronic density of states at the Fermi energy $N(E_F)$ and the electronic part of the specific heat (per unit temperature), γ. $N(E_F)$ is defined as

$$N(E_F) = \frac{1}{4\pi^3}\int_S \frac{dS}{|\nabla_k \epsilon|}, \qquad (2)$$

TABLE I. FS parameters obtained from reconstructed $\rho^{ep}_{\mathrm{LCW}}(\boldsymbol{k})$ compared with the LMTO calculation [6]. The uncertainty in the experimental values is $\sim$0.02 a.u.

FS sheet	Direction	Expt (a.u.)	Theory (a.u.)
Band 7	R-Γ	0.28	0.27
"	R-X	0.30	0.25
"	R-M	0.31	0.29
Band 6	Γ-M	0.16	0.14
"	Γ-X	0.19	0.2
"	Γ-R	0.13	No edge
"	X-M	0.08	0.068
"	X- Γ	0.11	0.07

where the integral is over the FS and $\gamma = N(E_F)\pi^2 k_B^2/3$. As Eq. (2) shows, $N(E_F)$ depends on the FS, experimentally available, and on the gradient of the energy function at $\boldsymbol{k}_F$, $\nabla_k \epsilon$, which is inaccessible to the 2D-ACAR experiment. One could adopt for $|\nabla_k \epsilon|$: (i) the free electron model expression ($|\nabla_k \epsilon| = \hbar^2 k_F/m$); (ii) the average gradient at $\epsilon(k_F)$ obtained from a band structure calculation. Either approximation would be unrealistic for heavy fermions, where the real energy dispersion can be exceedingly small compared to the one calculated via LDA. Conversely, the low cyclotron masses observed in $TmGa_3$ [6] suggest to adopt with some confidence the gradients obtained from the band structure calculation of Ref. [6] (see values reported above). We then obtain $\gamma \simeq 0.5$ mJ/(mole K^2) and $\gamma \simeq 1.9$ mJ/(mole K^2) for the electronlike and holelike FSs, respectively. It is clear that our estimates cannot take into account mass enhancements arising from electron-magnon or electron-phonon interaction and should simply be viewed as reference unenhanced values. The corresponding γ calculated via LDA for $TmGa_3$ and $LuGa_3$ were $\gamma \simeq 3.1$ mJ/(mole K^2) and $\gamma \simeq 2.87$ mJ/(mole K^2) [6], in fair agreement with our total $\gamma \simeq 2.4$ mJ/(mole K^2), corresponding to $N(E_F) =$ 13.6 states/Ryd cell.

Finally, we discuss the possible link between FS nesting and antiferromagnetism in $TmGa_3$. Indeed, a significant part of the holelike FS (see Fig. 2, nearby letter S, and Fig. 4) does show nesting features in the [110] directions. In Fig. 4, the translation which would cause the 1D sections of the FS to coincide is highlighted by an arrow. The extent of the spanning vector $\boldsymbol{q}_0$, is

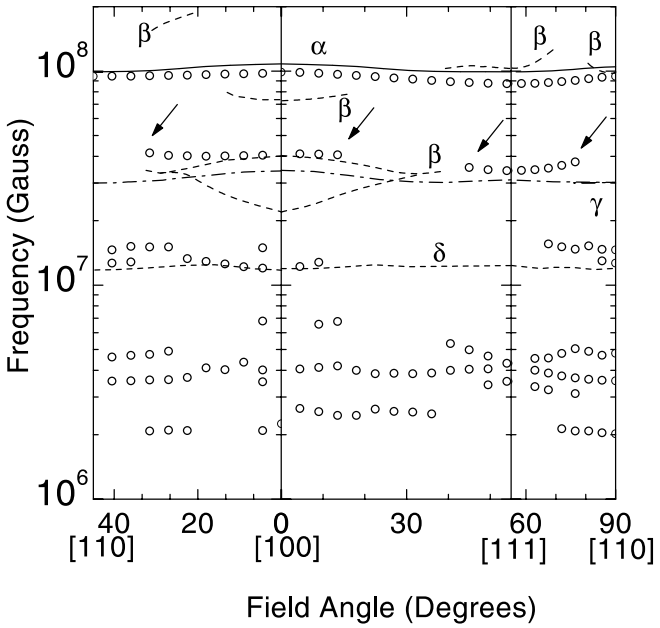

FIG. 3. Angular dependence of the dHvA frequencies pertaining to our reconstructed FS (continuous, dashed, and dot-dashed lines) compared to the dHvA frequencies (points) [6]. Note the interruption of one β dHvA branch marked by the arrows, as described in the text.

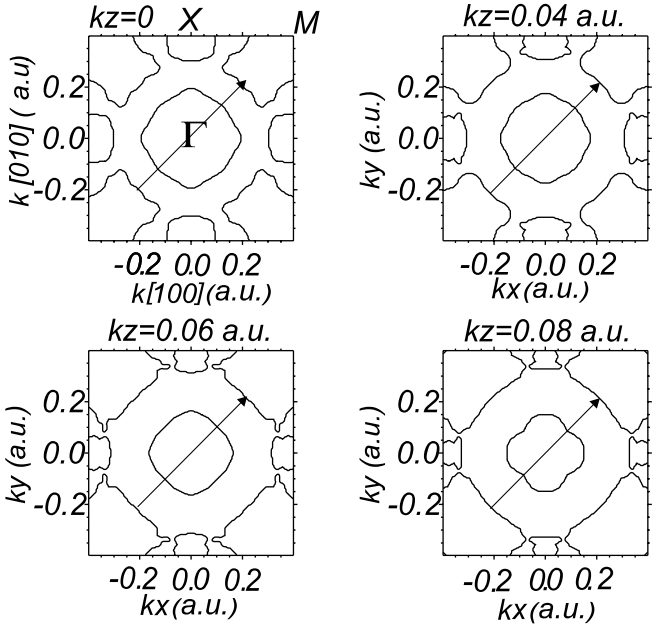

FIG. 4. Intersections of the experimental holelike FS with planes normal to [001] nearby the Γ point. The arrow highlights the FS nesting described in the text.

$q_0 = (0.59 \pm 0.02)$ a.u. [the reconstruction with the FBP method yields $q_0 = (0.57 \pm 0.02)$ a.u.]. This value is close to the distance $|\Gamma M| = 0.56$ a.u., corresponding to the propagation vector along [110] for commensurate antiferromagnetism. Obviously, the significance of the nesting feature is proportional to the extent of the region at interest. We estimated that area to be $\simeq(2 \times 0.19 \times 0.08)$ a.u.^{2}, equivalent to 5% of $(2\pi/a)^2$. We surmise that the antiferromagnetism of $TmGa_3$ is related to these features of the FS topology. One may wonder whether the small difference between spanning vector $\boldsymbol{q}_0$ and $|\Gamma M|$ is consistent with the commensurate antiferromagnetism of $TmGa_3$. In this regard, it is worth recalling the magnetic behavior of the isostructural system $ErGa_3$, where neutron measurements do observe incommensurate antiferromagnetism with $\boldsymbol{q} = [|\Gamma M| - \delta, |\Gamma M| - \delta, 0]$, and $\delta = 4\%$ [4,5]. The dHvA frequencies observed almost coincide with those of $TmGa_3$ although some low-frequency branches observed for $TmGa_3$ do not appear in the case of $ErGa_3$ [19]. An interesting question is whether the incommensurate antiferromagnetism of $ErGa_3$ can be linked to FS nesting as well. If our surmise is justified and within the limitations due to the experimental resolution one should observe an increase in the departure between a spanning vector $\boldsymbol{q}_0$ and $|\Gamma M|$ in $ErGa_3$. On the other hand, the FSs of the two compounds calculated by the f-core LDA methods [6,19] turn out to be almost identical as only the $5d^1$ and $6s^2$ electrons of the RE atoms are treated as itinerant. Therefore, one should attempt other methods to predict different FS nestings in the two compounds. In this regard, the self-interaction correction, known to increase the localization of the one electron spatial wave functions [20] or the "LDA + U" method, which aims at accounting for the strong on-site atomiclike correlation effects of the f electrons [21], could be employed to describe appropriately a small hybridization of the $4f$ electrons with the conduction electrons.

In conclusion, thanks to the accurate calipering of the FS of $TmGa_3$ we could address important electronic parameters such as γ constant and Fermi volume. Moreover, we put forward arguments in favor of FS driven antiferromagnetism.

We thank Dr. G. E. Grechnev for stimulating discussions and the State Committee for Scientific Research (Republic of Poland, Grant No. 2 P03B 083 16) for financial support.

*Also at Istituto Nazionale di Fisica della Materia, Corso Perrone 24, 16152 Genova, Italy.
†Permanent address: Departamento de Física, Universidad Carlos III, Avenida Universidad 30, 28911 Leganés (Madrid), Spain.

[1] See, for example, C. Kittel, *Solid State Physics,* edited by F. Seitz, D. Turnbull, and H. Ehrenreich (Wiley, New York, 1968), Vol. 22, p. 1.
[2] C. Herring, in *Magnetism,* edited by G. T. Rado and H. Suhl (Academic Press, Inc., New York, 1966), Vol. IV.
[3] D. Schmitt and P. M. Levy, J. Magn. Magn. Mater. **49**, 15 (1985).
[4] P. Morin, M. Giraud, P. L. Regnault, E. Roudaut, and A. Czopnik, J. Magn. Magn. Mater. **66**, 345 (1987).
[5] P. Morin, M. Giraud, P. Burlet, and A. Czopnik, J. Magn. Magn. Mater. **68**, 107 (1987).
[6] V. B. Pluzhnikov, A. Czopnik, G. E. Grechnev, N. V. Savchenko, and W. Suski, Phys. Rev. B **59**, 7893 (1999).
[7] A. Slebarski and A. Czopnik (to be published).
[8] S. Berko, *Positron Solid-State Physics,* edited by W. Brandt and A. Dupasquier (North-Holland, Amsterdam, 1983), p. 64.
[9] D. G. Lock, V. H. Crisp, and R. N. West, J. Phys. F **3**, 561 (1973).
[10] J. H. Kaiser, R. N. West, and N. Shiotani, J. Phys. F **16**, 1307 (1986).
[11] A. Rubaszek, Z. Szotek, and W. M. Temmerman, Phys. Rev. B **58**, 11 285 (1998).
[12] C. K. Majumdar, Phys. Rev. A **140**, 227 (1965).
[13] M. Biasini *et al.,* J. Phys. Condens. Matter **12**, 5961 (2000).
[14] U. Gerhardt, S. Marquardt, N. Schroeder, and S. Weiss, Phys. Rev. B **58**, 6877 (1998).
[15] A. M. Cormack, J. Appl. Phys. **35**, 2908 (1964).
[16] G. Kontrym-Sznajd, Phys. Status Solidi (a) **79**, 227 (1990).
[17] G. Kontrym-Sznajd and E. Jozefczuk, Mater. Sci. Forum **255–257**, 754 (1997), and references therein.
[18] S. B. Dugdale *et al.,* Phys. Rev. Lett. **79**, 941 (1997).
[19] V. B. Pluzhnikov, A. Czopnik, and G. E. Grechnev, J. Phys. Condens. Matter **11**, 4507 (1999).
[20] J. P. Perdew and A. Zunger, Phys. Rev. B **23**, 5048 (1981); A. Svane and O. Gunnarsson, Phys. Rev. Lett. **65**, 1148 (1990).
[21] A. B. Shick, A. I. Liechtenstein, and W. E. Pickett, Phys. Rev. B **60**, 10 763 (1999).